JOC The Journal of Organic Chemistry Cite This: J. Org. Chem. XXXX, XXX, XXX−XXX

Note

pubs.acs.org/joc

Intramolecular [2 + 2] Photocycloaddition of Altrenogest: Confirmation of Product Structure, Theoretical Mechanistic Insight, and Bioactivity Assessment

Nicholas C. Pflug,*[,†] Eric V. Patterson,[‡] Dalma Martinović-Weigelt,[§] Edward P. Kolodziej,[∥,⊥] James B. Gloer,[#] Kristopher McNeill,[†] David M. Cwiertny,[▽] and Kristine H. Wammer[○]

[†]Institute of Biogeochemistry and Pollutant Dynamics, ETH Zurich, 8092 Zurich, Switzerland

[‡]Department of Chemistry, Stony Brook University, Stony Brook, New York 11794, United States

[§]Department of Biology, University of St. Thomas, St. Paul, Minnesota 55105, United States

[∥]Interdisciplinary Arts and Sciences, University of Washington, Tacoma, Tacoma, Washington 98402, United States

[⊥]Department of Civil and Environmental Engineering, University of Washington, Seattle, Washington 98195, United States

[#]Department of Chemistry, University of Iowa, Iowa City, Iowa 52242, United States

[▽]Department of Civil and Environmental Engineering, University of Iowa, Iowa City, Iowa 52242, United States

[○]Department of Chemistry, University of St. Thomas, St. Paul, Minnesota 55105, United States

Supporting Information

While studying the environmental fate of potent endocrine-active steroid hormones, we observed the formation of an intramolecular [2 + 2] photocycloaddition product (**2**) with a novel hexacyclic ring system following the photolysis of altrenogest (**1**). The structure and absolute configuration were established by X-ray diffraction analysis. Theoretical computations identified a barrierless two-step cyclization mechanism for the formation of **2** upon photoexcitation. **2** exhibited progesterone, estrogen, androgen, and pregnane X receptor activity, albeit generally with reduced potency relative to **1**.

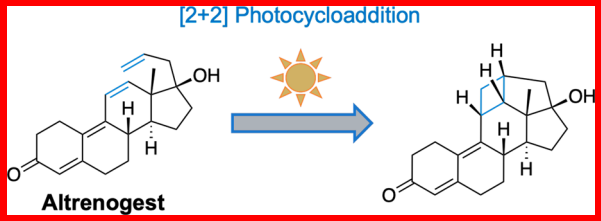

Altrenogest (**1**) is a potent, synthetic progestin widely used in animal agriculture for synchronizing estrus (i.e., heat) in pigs and horses under trade names including Regu-Mate and Matrix (both available through Merck Animal Health) or Altresyn (Ceva).[1−3] For estrous synchronization, swine receive 210−360 mg doses of **1** over 12−18 days, whereas in horses, 230−400 mg is used over 15 days.[4,5] **1** is also used for pregnancy maintenance in horses, where >7000 mg total may be administered over the 300+ day gestation period.[6] As global dietary patterns shift toward the increasing consumption of protein, a more widespread and rapidly increasing use of **1** is likely as pork production intensifies to meet growing demand, particularly under the market strain from African swine fever.[7,8] Because synthetic progestins have been shown to induce adverse impacts on aquatic ecosystems at even trace (parts per trillion or nanograms per liter) levels, robust environment monitoring will be necessary to track the occurrence, fate, and impact of **1** in water and soil systems.[9−12] Indeed, it is reasonable to expect a significant release of **1** into the environment due to its incomplete metabolism, with excretion in feces that is often used as fertilizer through the land application of manure.[13]

Despite its increasingly widespread use and potent endocrine-disrupting potential, remarkably little work has been conducted, either in the laboratory or in the field, related to the environmental fate and effects of **1**. This could be due in part to the photochemical reactivity we previously observed when examining the fate of **1** in sunlit surface waters.[14] Under simulated sunlight, we observed a rapid photoisomerization of **1** to a product whose structure we previously proposed as **2** based on 2D nuclear magnetic resonance (NMR) analysis, which could form via an intramolecular [2 + 2] cycloaddition reaction.[14] Several aspects of this reaction complicate studies of the environmental fate and effects of **1**. First, it is very fast, with a half life on the order of several seconds under normal daylight irradiation conditions. Second, it yields an isomeric product, complicating the accurate quantification of **1** in environmental samples solely based on mass spectrometry analysis. Third, an intramolecular [2 + 2] cycloaddition is an atypical photoreaction for steroidal hormones yet would still yield a product with features that could retain bioactivity and therefore pose an ecosystem risk. Collectively, these issues may confound otherwise routine experiments and the analysis of environmental samples of **1**. For example, in a recent pharmacokinetic study of the intrarectal administration of **1** in horses, evidence of **2** was found in some blood plasma samples

Received: July 29, 2019
Published: August 5, 2019

DOI: 10.1021/acs.joc.9b02070

from treated horses, presumably formed during handling and the application of **1** through incidental exposure to light.[15]

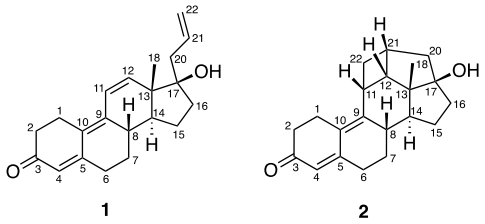

1 **2**

Given the complexities of the **1** system, more work is needed to establish and validate the photoproduct while also attempting to characterize the nature of the [2 + 2] cycloaddition reaction. Herein we provide X-ray crystallographic analysis to confirm the structure of **2**. We also conduct computational chemical studies to explore the thermodynamic driving force for the formation of **2** in an attempt to rationalize the fast photochemical process that yields an unprecedented, seemingly strained product. Finally, we previously found **2** to exhibit androgen receptor (AR) activity, whereas additional in silico 3D receptor docking models for **2** predict substantial retained affinity for the progesterone receptor (PR).[14] Guided by these prior in silico modeling results, we also use commercial nuclear receptor activation assays to explore a broader suite of nuclear receptor end points for **2**.

We emphasize that unambiguously establishing the bioactivity of **1** and **2** is of utmost importance not only for ecological receptors but also for human health for those that administer **1** to animals. Indeed, in July 2018, the U.S. Food and Drug Administration released a warning regarding a series of observations of human health impacts arising from incidental exposure to **1**, citing adverse reproductive effects in women and girls, including abnormal or absent menstrual cycles, and in men, including decreased libido.[16] Given the retained bioactivity we previously reported for **2** and the ease with which it is generated, including in drug formulations,[14] there is a potential for additional or distinct adverse health outcomes from exposure to **2**.

Confirmation of Structure and Absolute Configuration. A sample of **2** was generated (~96% isolated yield) by irradiating a solution of **1** with UV-A light (350−400 nm). Single-crystal X-ray diffraction analysis using Cu Kα radiation confirmed the proposed structure of **2**, and a perspective ORTEP plot is shown in Figure 1. The value of the Flack parameter, −0.08 (6), allowed the assignment of the 8*S*, 11*R*, 12*S*, 13*R*, 14*S*, 17*R*, 21*R* absolute configuration, which verified that no stereochemical change had occurred at stereocenters initially present in **1**. To our knowledge, apart from our initial proposal,[14] no compound having the hexacyclic core structure (or tetracyclic 6,5,5,4-subunit) shown in **2** has been previously reported in the literature as either a synthetic or natural product.

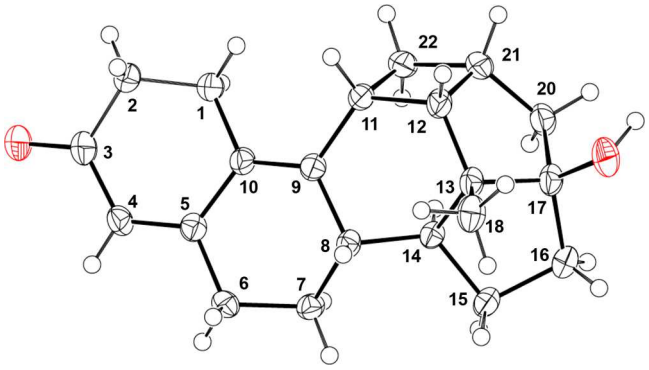

Figure 1. Thermal ellipsoid representation of **2**. Ellipsoids are depicted at 50% probability.

Theoretical Mechanistic Modeling. Upon photoexcitation, **1** is known to form a triplet state.[14] We therefore initially modeled the ring closure on the T_1 surface using relaxed scans. (See the SI.) Vertical excitation forms a stabilized diradical within the trienone moiety with significant radical density on C-12 in close physical proximity to the C-17 allyl chain. This primes the system for a facile C-12/C-21 closure. We identified a two-step mechanism involving the stepwise closure of first the C-12/C-21 bond to form a diradical intermediate, followed by the closure of the C-11/C-22 bond to **2**. We could find no evidence of a concerted pathway. Stationary points were optimized based on the scan data (**1**, **TS1**, **INT**, **TS2**, and **2**). The geometries and relative energies of these stationary points are virtually identical at both the density functional theory (DFT) and MRPT2//CAS levels employed (Table 1).

Table 1. Relative Energies (kcal/mol) for Stationary Points in the [2 + 2] Cycloaddition of 1 to 2[a]

	DFT			
	reaction coordinate[b]	S_0	S_0 S^2	T_1
1	7.12	0	0.00	36
TS1	5.08	37	0.94	48
INT	4.44	30	1.07	29
TS2	3.95	34	0.88	55
2	3.12	−5	0.00	43
	MRPT2//CAS			
	reaction coordinate[b]	S_0	S_0 HOMO/LUMO occupancy	T_1
1	7.54	0	1.87/0.14	44
TS1	5.22	36	1.40/0.60	51
MEX 1 (T_1/S_0)	4.81	41	1.03/0.98	41
INT	4.59	40	1.08/0.93	40
MEX 2 (T_1/S_0)	4.54	40	1.05/0.96	40
TS2	4.11	36	1.52/0.48	N/A[c]
2	3.18	0	1.89/0.13	55

[a]DFT values are solvated relative free energies at the M11/def2-TZVP + SMD level or broken-symmetry UM11/def2-TZVP + SMD level. MRPT2//CAS values are relative electronic energies at the MRPT2//CAS(10,10)/cc-pVDZ level. [b]Reaction coordinate is defined as the sum of the C12−C21 and C11−C22 bond distances. [c]No attempt was made to optimize **TS2** at the CAS level because we predict that the reaction returns to the S_0 surface prior to **TS2**.

We explored the same pathway on the S_0 surface, allowing for the formation of open-shell diradical singlet states by employing broken-symmetry unrestricted density functional theory (UDFT) calculations wherein the α and β orbitals are mixed. In the region between **TS1** and **TS2**, S^2 of the UDFT wave functions are all near 1, which indicates an open-shell singlet wave function (Table 1). This observation was confirmed by MRPT2//CAS calculations. It was also found that the S_0 and T_1 surfaces are degenerate in the transition region. In fact, two minimum energy crossing points between T_1 and S_0 were found at the MRPT2//CAS level, one immediately prior to **INT** and one immediately after. Collectively, the DFT and MRPT2//CAS data paint a picture of a very flat diradical surface between **TS1** and **TS2** where S_0 and T_1 are virtually indistinguishable.

DOI: 10.1021/acs.joc.9b03079

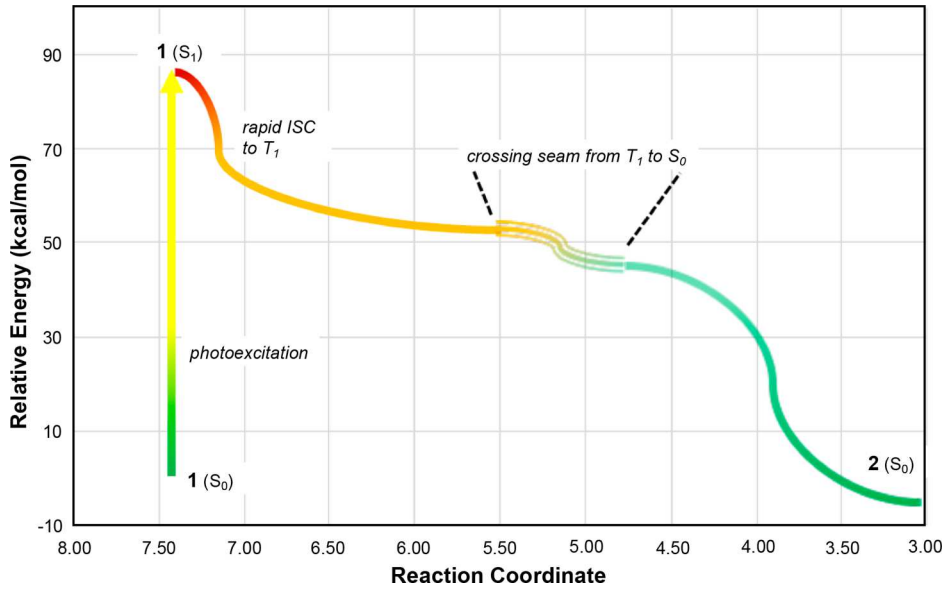

Figure 2. Proposed reaction energy diagram for the [2 + 2] cycloaddition of **1** to **2**, showing the initial vertical excitation to S_1, followed by the sequential crossing to T_1 then S_0.

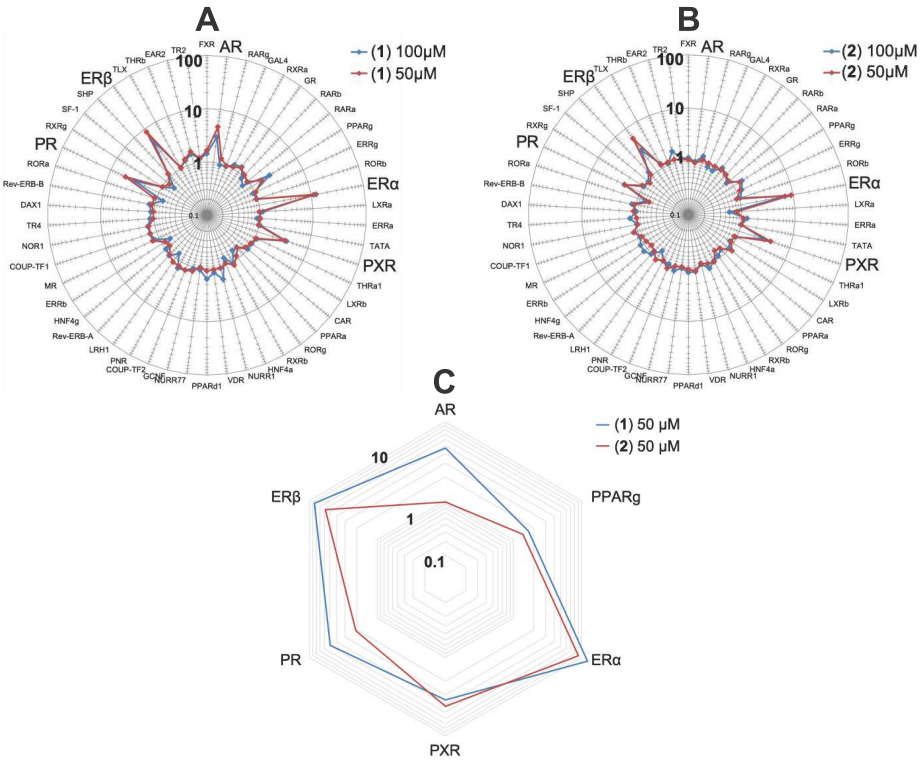

Figure 3. Effect of (A) **1** and (B) **2** on the activity of 48 human nuclear receptors in HepG2 cells and (C) effect of **1** and **2** on human nuclear receptors that were found to be activated two times or more relative to vehicle-treated controls. Activities are expressed as fold-induction values versus vehicle-treated control cells. Graphs show mean fold-induction data (n = 3) plotted on a logarithmic scale.

Given the essentially degenerate nature of the transition region of the reaction coordinate, we present the following pathway for the transformation of **1** to **2**. Initial photoexcitation (λ_{max} = 350 nm exp, 323 nm time-dependent density functional theory (TD-DFT)) within the conjugated π system of **1** to S_1 is followed by rapid intersystem crossing (ISC) to the triplet manifold (Figure 2). The T_1 surface intersects the S_0 surface at or near **TS1**, and the two surfaces remain degenerate throughout the closure, facilitating relaxation back to the S_0 surface. Because **TS1**, **INT**, and **TS2** are nearly isoenergetic, we predict a mechanism that is technically two steps but functions as an asynchronous single-step closure. In other words, there is no barrier to complete the closure following photoexcitation. During the final closure, degeneracy is broken and S_0 collapses to **2** (Figure 2).

Our computational data fully support a rapid and irreversible photocatalyzed cycloaddition from **1** to **2**. Whereas both **1** (λ_{max} = 350 nm) and **2** (λ_{max} = 320 nm) absorb in the solar spectrum, it

DOI: 10.1021/acs.joc.9b03070

is the dienone moiety in **2** that is the chromophore, and the generation of a diradical excited state in the chromophore will not lead to the cleavage of the newly formed σ bonds. Indeed, the excited state of **2** is known to rapidly photohydrate while retaining its cyclized structure.[14] Reversion to **1** in the photoexcited state is therefore highly unlikely under ambient conditions. The forward and reverse thermal barriers both exceed 40 kcal/mol, making the thermal process inaccessible at ambient temperatures.

There are a few discrepancies in relative energies between the two theoretical methods employed. However, the differences observed are minor and reasonable given the fundamental differences between single-reference DFT and multireference MRPT2//CAS. The latter is likely to be less accurate for the **1**/**2** gap due to the significant change in the character of the active space orbitals, and this is indeed where the largest discrepancy is seen. We note that single-point MP2 and CCSD calculations confirm that **2** is indeed lower in energy than **1**. (See the SI.) Importantly, the conclusions are not affected by these discrepancies. We predict the reaction to be rapid and irreversible regardless of the precise energy differences among the various stationary points.

Biological Activity Assessment. Samples of **1** (positive control) and **2** tested at 50 and 100 μM in triplicate were screened against 48 human nuclear receptors (hNRs) using a commercially available cellular biosensor system (trans-FACTORIAL assays, Attagene, Morrisville, NC[17,18]). Product **2** retained two times or higher agonistic activity relative to vehicle-treated control cells for four of the six hNRs upregulated by **1** (i.e., estrogen receptor (ER) α and β, PR, and pregnane X receptor (PXR); Figure 3). For example, at 50 μM, **1** was observed to activate PR, ERα, ERβ, and PXR with 4.9 ± 0.6, 12.4 ± 1.1, 8.5 ± 0.6, and 3.5 ± 0.4 mean fold-induction values, whereas **2** was observed to retain activity at the same receptors, but with ~45, 75, 70, and 100% of the activity, respectively.

Past virtual ligand screening[14] predicted that **2** would activate PR and AR. Given the observed lack of AR activation and strong activation of ER by **2** in the trans-FACTORIAL assay, we conducted a further analysis of **1** and **2** with traditional AR and ERα transcriptional activation assays (Indigo Biosciences, State College, PA) that have excellent sensitivity and a dynamic range and are thus more suitable for quantifying relative potency. The activation of ERα by both **1** and **2** was confirmed, but their potencies were very low; EC_{10} values for **1** and **2** were in the millimolar range, whereas EC_{10} for 17β-estradiol was 30 pM. (See the SI.) Both **1** and **2** also exhibited androgenic activity in the traditional transcriptional activation assay (see the SI), with estimated EC_{50} values of 122 and 166 nM, respectively. The retention of androgenic activity by **2** is congruent with the in silico predictions and the results obtained by another traditional in vitro transcriptional assay, MDA-kb2.[14]

Environmental Implications. The activation of ER is unlikely to be environmentally relevant given the low estrogenic potency of both **1** and **2**. However, the newly demonstrated PR activation by **2** is notable because **1** has been reported to be ~13 times more potent than the endogenous PR ligand progesterone.[19] The agonism of **1** and **2** for AR and PXR is also of concern given the biological roles of these receptors (i.e., reproduction and hepatic energy metabolism,[20] respectively). Further characterization of the relative in vivo potency is warranted.

We have previously identified a photohydration (in light)-thermal dehydration (in dark) diurnal cycling for **2**, which is expected to increase its persistence in sunlit surface waters despite the appearance of attenuation.[14] This is expected to maintain ecosystem and human health risks associated with the inevitable release of **1** to the environment or incidental exposure during handling and administration to animals. Collectively, our results underscore the need for more comprehensive fate and risk assessment profiling, including prioritization of environmental transformation products for high-potency pollutant classes such as endocrine-disrupting steroids.

EXPERIMENTAL SECTION

Reagents. The experiments used Altrenogest (Sigma, ≥98%), acetonitrile-d_3 (Armar, 99.8 atom % D), nanopure water (resistivity >18 MΩ cm), acetonitrile (Fisher Scientific, ≥99.9%), absolute ethanol (VWR Chemicals, ACS reagent grade), and *n*-hexane (Merck Millipore; LC-MS hypergrade).

Photogeneration of 2. Twenty-five mg (0.081 mmol) of **1** was dissolved in 1 mL of acetonitrile-d_3, and the solution was added to a Schlenk NMR tube, sealed, and degassed using the freeze−pump−thaw method (three times). The solution was photolyzed with a commercially available Rayonet photoreactor (The Southern New England Ultraviolet Company, Branford, CT) equipped with six UV-A (350−400 nm) bulbs until **1** was observed to be completely transformed to **2** (~25 min) by ^{1}H NMR. (See Figures S1 and S2 for the spectrum and our previous work for assignments.[14]) Purification by reverse-phase semipreparative high-performance liquid chromatography (HPLC) afforded **2** (24.1 mg, ~96% isolated yield). ^{1}H NMR (CD_3CN, 400 MHz): δ 0.88 (s, 3H), 1.21 (ddd, 1H, J = 18.2, 12.1, 6.1 Hz), 1.52 (ddd, 1H, J = 12.8, 7.1, 6.2 Hz), 1.59−1.78 (m, 3H), 1.85 (dq, 1H, J = 12.4, 3.6 Hz), 2.01−2.12 (m, 2H), 2.16−2.56 (m, 9H), 2.61−2.85 (m, 3H), 2.97 (tdd, 1H, J = 11.5, 9.6, 1.5 Hz), 3.50 (dt, 1H, J = 10.7, 7.8 Hz), 5.57 (s, 1H). ^{13}C{^{1}H} NMR (CD_3CN, 100 MHz): δ 12.9, 24.9, 25.5, 29.2, 31.8, 32.0, 34.1, 37.0, 37.4, 38.5, 41.5, 46.6, 49.1, 53.2, 53.8, 94.7, 122.3, 126.1, 153.9, 157.8, 199.2. HRMS (ESI/ion trap) m/z: $[M + H]^+$ Calcd for $C_{21}H_{27}O_2$ 311.2011; Found 311.2016.

Analytical Methods. *High-Performance Liquid Chromatography.* **2** was purified with a Thermo Scientific Dionex Ultimate 3000 HPLC-Variable wavelength detector system equipped with a Supelco Ascentis-C_{18} (10 × 250 mm, 5 μm) column using 50/50 acetonitrile/water isocratic elution (2 mL/min), 320 nm wavelength detection, and Chromeleon 7 analysis software.

Nuclear Magnetic Resonance Spectroscopy. ^{1}H and ^{13}C NMR data were recorded using a Bruker AVANCE-400 spectrometer with acetonitrile-d_3 as the solvent. Chemical shift values were referenced to the residual solvent signal (δ_H/δ_C 1.94/118.26 CD_3CN), and NMR data were processed using Bruker Topspin 3.5 software.

High-Resolution Mass Spectrometry. HRMS data were recorded using a Thermo Exactive Orbitrap mass spectrometer with an electrospray ionization source operated in positive ionization mode. Thermo Xcalibur software was used for data acquisition and processing.

X-ray Crystallographic Analysis. Colorless crystals of **2** were obtained from *n*-hexane−ethanol (10:1) using the vapor diffusion method. A suitable crystal (0.425 × 0.110 × 0.069 mm) was selected and used for X-ray crystallographic analysis. The X-ray intensity data were measured with a Rigaku Oxford Diffraction XtalLAB Synergy Dualflex Pilatus 300 K diffractometer using Cu Kα radiation. The crystal was kept at 100.0 K during data collection. Using Olex2, the structure was solved with the ShelXT structure solution program using intrinsic phasing and refined with the ShelXT refinement package using least-squares minimization. Crystal Data: hexagonal, space group $P6_5$ (no. 170), a = 15.63070(10) Å, c = 12.53510(10) Å, V = 2652.25(4) Å^3, Z = 6, T = 100.0(1) K, μ(Cu Kα) = 0.603 mm^{-1}, D_{calc} = 1.200 g/cm^3, 70 373 reflections measured ($9.616 \leq 2\Theta \leq 159.066°$), 3711 unique ($R_{int}$ = 0.0425, R_{sigma} = 0.0121), which were used in all calculations. The final R_1 was 0.0349 ($I > 2\sigma(I)$), and wR_2 was 0.0948 (all data). Atomic coordinates for compound **2** have been deposited with the Cambridge Crystallographic Data Centre (deposition number 1914885).

Theoretical Computations. The [2 + 2] ring closure of **1** to **2** was modeled using quantum-mechanical DFT and multiconfigurational CAS and MRPT2 methods. The M11 density functional[21] was chosen

DOI: 10.1021/acs.joc.9b03070

for its good general performance. A CAS(10,10) active space was chosen, composed of the π/π^* system in **1**, which morphs into the π/π^* system in **2** along with the two new σ/σ^* bonds. The def2-TZVP basis set[22] and aqueous SMD continuum solvation model[23] were used for all DFT calculations. The cc-pVDZ basis set[24] was used for the multiconfigurational calculations.

At the DFT level, unrestricted broken-symmetry calculations (e.g., with α/β mixing) were used to approximate open-shell singlet states on the S_0 surface, allowing the determination of a complete mechanistic pathway from **1** to **2** on the S_0 surface. Given that a triplet state is known from photoexcitation, the analogous T_1 pathway was also determined. All stationary points were characterized as minima or transition states according to normal-mode analysis. Intrinsic reaction coordinate (IRC) calculations were used to confirm each transition state. All stationary point energies were corrected to Gibbs free energies under standard conditions of 298.15 K and 1 M solution. Single-point TD-DFT calculations were used to determine vertical $S_0 \rightarrow S_1$ transitions at selected points.

Corresponding stationary points were determined on the S_0 and T_1 surfaces at the CAS(10,10)/cc-pVDZ level. Minimum energy crossing points were found between the two surfaces. Single-point MRPT2 calculations[25] were performed on all stationary points. MRPT2 electronic energies were used without correction because the exploration at the DFT level revealed a small influence of thermodynamic corrections on relative energies and no effect from solvation corrections.

DFT calculations were performed using Gaussian 16,[26] whereas GAMESS[27] was used for the multiconfigurational studies.

Bioassays. For the Attagene trans-FACTORIAL hNR assay, see the method described by Romanov et al.[18] For in vitro human ERα and AR reporter assays, **1** and **2** were prepared in 100% DMSO, diluted in the assay media provided by the manufacturer (to ensure that DMSO concentrations in the assay were below 0.01%), and tested in duplicate at six different concentrations ranging from 2.5×10^{-5} to 7.81×10^{-12} M (20× dilution series). The EC_{10} and EC_{50} values for the assay-specific positive control (17β-estradiol and 6α-fluoro-testosterone) and for **1** and **2** were calculated using nonlinear regression (log agonist vs response - three parameters; Prism 5.02. Graph Pad Software, La Jolla, CA).

■ ASSOCIATED CONTENT

Supporting Information

The Supporting Information is available free of charge on the ACS Publications website at DOI: 10.1021/acs.joc.9b02070.

^{1}H and ^{13}C NMR spectra of **2**, HRMS chromatogram of **2**, and X-ray crystallography data, computational scan data, relative energies, single-point calculations, active space orbitals, coordinates, and nuclear receptor dose−response curves (PDF)

Crystallographic data for **2** (CIF)

■ AUTHOR INFORMATION

Corresponding Author

*E-mail: nicholas.pflug@usys.ethz.ch.

ORCID

Nicholas C. Pflug: 0000-0002-2023-2162
Edward P. Kolodziej: 0000-0002-7968-4198
James B. Gloer: 0000-0002-9261-7571
Kristopher McNeill: 0000-0002-2981-2227
David M. Cwiertny: 0000-0001-6161-731X

Notes

The authors declare no competing financial interest.

■ ACKNOWLEDGMENTS

Support for this work from the U.S. NSF (CHE-1609791 and CHE-1335711 to D.M.C. and N.C.P., CHE-1662030 to E.V.P., CHE-1609669 and CHE-1229354 to the MERCURY consortium, and CBET-1336165 to D.M.-W.) and ETH Zurich is gratefully acknowledged. We thank Dr. Nils Trapp of the Small Molecule Crystallography Center at ETH Zurich for X-ray crystallographic analysis.

■ REFERENCES

(1) Squires, E. L.; Heesemann, C. P.; Webel, S. K.; Shideler, R. K.; Voss, J. L. Relationship of altrenogest to ovarian activity, hormone concentrations and fertility of mares. *J. Anim. Sci.* **1983**, *56*, 901.

(2) van Leeuwen, J. J. J.; Williams, S. I.; Martens, M. R. T. M.; Jourquin, J.; Driancourt, M. A.; Kemp, B.; Soede, N. M. The effect of postweaning altrenogest treatments of primiparous sows on follicular development, pregnancy rates, and litter sizes. *J. Anim. Sci.* **2011**, *89*, 397.

(3) Willmann, C.; Schuler, G.; Hoffmann, B.; Parvizi, N.; Aurich, C. Effects of age and altrenogest treatment on conceptus development and secretion of LH, prosgesterone, and eCG in early-pregnant mares. *Theriogenology* **2011**, *75*, 421.

(4) Regu-Mate Product Label. https://www.merck-animal-health-usa.com/product/equine/Regu-Mate-Solution/1 (accessed July 1, 2019).

(5) Estienne, M. J.; Harper, A. F.; Horsley, B. R.; Estienne, C. E.; Knight, J. W. Effects of P.G. 600 on the onset of estrus and ovulation rate in gilts treated with Regu-mate. *J. Anim. Sci.* **2001**, *79*, 2757.

(6) Squires, E. L. Hormonal manipulation of the mare: a review. *J. Equine Vet. Sci.* **2008**, *28*, 627−634.

(7) Sánchez-Cordón, P. J.; Montoya, M.; Reis, A. L.; Dixon, L. K. African swine fever: A re-emerging viral disease threatening the global pig industry. *Vet. J.* **2018**, *233*, 41−48.

(8) Brown, V. R.; Bevins, S. N. A review of African Swine Fever and the potential for introduction into the United States and the possibility of subsequent establishment in feral swine and native ticks. *Front. Vet. Sci.* **2018**, *5*, 1−18.

(9) Zucchi, S.; Castiglioni, S.; Fent, K. Progestins and antiprogestins affect gene expression in early development in Zebrafish (*Danio rerio*) at environmental concentrations. *Environ. Sci. Technol.* **2012**, *46*, 5183−5192.

(10) Zeilinger, J.; Steger-Hartmann, T.; Maser, E.; Goller, S.; Vonk, R.; Länge, R. Effects of synthetic gestagens on fish reproduction. *Environ. Toxicol. Chem.* **2009**, *28*, 2663−2670.

(11) Fent, K. Progestins as endocrine disrupters in aquatic ecosystems: Concentrations, effects and risk assessment. *Environ. Int.* **2015**, *84*, 115−130.

(12) Runnalls, T. J.; Beresford, N.; Losty, E.; Scott, A. P.; Sumpter, J. P. Several synthetic progestins with different potencies adversely affect reproduction of fish. *Environ. Sci. Technol.* **2013**, *47*, 2077−2084.

(13) Lampinen-Salomonsson, M.; Beckman, E.; Bondesson, U.; Hedeland, M. Detection of altrenogest and its metabolites in post administration horse urine using liquid chromatography tandem mass spectrometry—increased sensitivity by chemical derivatisation of the glucuronic acid conjugate. *J. Chromatogr. B: Anal. Technol. Biomed. Life Sci.* **2006**, *833*, 245−256.

(14) Wammer, K. H.; Anderson, K. C.; Erickson, P. R.; Kliegman, S.; Moffatt, M. E.; Berg, S. M.; Heitzman, J. A.; Pflug, N. C.; McNeill, K.; Martinovic-Weigelt, D.; Abagyan, R.; Cwiertny, D. M.; Kolodziej, E. P. Environmental photochemistry of altrenogest: photoisomerization to a bioactive product with increased environmental persistence via reversible photohydration. *Environ. Sci. Technol.* **2016**, *50*, 7480−7488.

(15) Ellis, K. E.; Council-Troche, R. M.; Von Dollen, K. A.; Beachler, T. M.; Bailey, C. S.; Davis, J. L.; Lyle, S. K. Pharmacokinetics of intrarectal altrenogest in horses. *J. Equine Vet. Sci.* **2019**, *72*, 41−46.

(16) FDA Animal Drug Safety Communication: FDA Highlights Potential Health Risks to People Exposed to Altrenogest Products for Horses or Pigs. https://www.fda.gov/animal-veterinary/cvm-updates/

fda-animal-drug-safety-communication-fda-highlights-potential-health-risks-people-exposed (accessed July 1, 2019).
(17) Martin, M. T.; Dix, D. J.; Judson, R. S.; Kavlock, R. J.; Reif, D. M.; Richard, A. M.; Rotroff, D. M.; Romanov, S.; Medvedev, A.; Poltoratskaya, N.; et al. Impact of environmental chemicals on key transcription regulators and correlation to toxicity end points within EPA's ToxCast program. *Chem. Res. Toxicol.* **2010**, *23*, 578−590.
(18) Romanov, S.; Medvedev, A.; Gambarian, M.; Poltoratskaya, N.; Moeser, M.; Medvedeva, L.; Gambarian, M.; Diatchenko, L.; Makarov, S. Homogenous reporter system enables quantitative functional assessment of multiple transcription factors. *Nat. Methods* **2008**, *5*, 253−260.
(19) McRobb, L.; Handelsman, D. J.; Kazlauskas, R.; Wilkinson, S.; McLeod, M. D.; Heather, A. K. Structure-activity relationships of synthetic progestins in a yeast-based in vitro androgen bioassay. *J. Steroid Biochem. Mol. Biol.* **2008**, *110*, 39−47.
(20) Hakkola, J.; Rysa, J.; Hukkanen, J. Regulation of hepatic energy metabolism by the nuclear receptor PXR. *Biochim. Biophys. Acta, Gene Regul. Mech.* **2016**, *1859*, 1072−1082.
(21) Peverati, R.; Truhlar, D. G. Improving the accuracy of hybrid meta-GGA density functionals by range separation. *J. Phys. Chem. Lett.* **2011**, *2*, 2810−2817.
(22) Weigend, F.; Ahlrichs, R. Balanced basis sets of split valence, triple zeta valence and quadruple zeta valence quality for H to Rn: design and assessment of accuracy. *Phys. Chem. Chem. Phys.* **2005**, *7*, 3297−3305.
(23) Marenich, A. V.; Cramer, C. J.; Truhlar, D. G. Universal solvation model based on solute electron density and on a continuum model of the solvent defined by the bulk dielectric constant and atomic surface tensions. *J. Phys. Chem. B* **2009**, *113*, 6378−6396.
(24) Dunning, T. H., Jr. Gaussian basis sets for use in correlated molecular calculations. I. The atoms boron through neon and hydrogen. *J. Chem. Phys.* **1989**, *90*, 1007−1023.
(25) Hirao, K. Multireference Møller-Plesset method. *Chem. Phys. Lett.* **1992**, *190*, 374−380.
(26) Frisch, M. J.; Trucks, G. W.; Schlegel, H. B.; Scuseria, G. E.; Robb, M. A.; Cheeseman, J. R.; Scalmani, G.; Barone, V.; Petersson, G. A.; Nakatsuji, H.; Li, X.; Caricato, M.; Marenich, A. V.; Bloino, J.; Janesko, B. G.; Gomperts, R.; Mennucci, B.; Hratchian, H. P.; Ortiz, J. V.; Izmaylov, A. F.; Sonnenberg, J. L.; Williams-Young, D.; Ding, F.; Lipparini, F.; Egidi, F.; Goings, J.; Peng, B.; Petrone, A.; Henderson, T.; Ranasinghe, D.; Zakrzewski, V. G.; Gao, J.; Rega, N.; Zheng, G.; Liang, W.; Hada, M.; Ehara, M.; Toyota, K.; Fukuda, R.; Hasegawa, J.; Ishida, M.; Nakajima, T.; Honda, Y.; Kitao, O.; Nakai, H.; Vreven, T.; Throssell, K.; Montgomery, J. A., Jr.; Peralta, J. E.; Ogliaro, F.; Bearpark, M. J.; Heyd, J. J.; Brothers, E. N.; Kudin, K. N.; Staroverov, V. N.; Keith, T. A.; Kobayashi, R.; Normand, J.; Raghavachari, K.; Rendell, A. P.; Burant, J. C.; Iyengar, S. S.; Tomasi, J.; Cossi, M.; Millam, J. M.; Klene, M.; Adamo, C.; Cammi, R.; Ochterski, J. W.; Martin, R. L.; Morokuma, K.; Farkas, O.; Foresman, J. B.; Fox, D. J. *Gaussian 16*, Revision A.03; Gaussian, Inc.: Wallingford, CT, 2016.
(27) Schmidt, M. W.; Baldridge, K. K.; Boatz, J. A.; Elbert, S. T.; Gordon, M. S.; Jensen, J. H.; Koseki, S.; Matsunaga, N.; Nguyen, Kiet A.; Su, Shujun; Windus, Theresa L.; Dupuis, Michel; Montgomery, John A. General atomic and molecular electronic structure system. *J. Comput. Chem.* **1993**, *14*, 1347−1363.

DOI: 10.1021/acs.joc.9b03070